Stability investigation of micro-configured Pd-Ag membrane modules – effect of operating temperature and pressure

T.A. Peters*, M. Stange, M.F. Sunding, and R. Bredesen

SINTEF Materials and Chemistry, P.O. Box 124 Blindern, N-0314, Oslo, Norway

* To whom correspondence should be addressed. E-mail: thijs.peters@sintef.no

Abstract

The long-term stability over a period of up to 50 days has been reported for various designs of microstructured $Pd_{77}Ag_{23}$ membrane modules for H_2 production and purification. Even though microchannels provide sufficient mechanical support for moderate trans-membrane pressure difference and temperatures, *i.e.*, 4–5 bars and 400–450 °C, long-term operation under these operating conditions results in a large deformative settling of the $Pd_{77}Ag_{23}$ film into the microchannel support. This settling leads to microstructural changes and pore formation on the feed surface of the membrane film that ultimately results in membrane failure. For pressures above approximately 5 bars, the application of microchannel-supported modules is thus not feasible, and for that purpose a continuous porous stainless steel support is introduced that allows for a sufficient stabilisation of the thin $Pd_{77}Ag_{23}$ films. For such a porous stainless steel supported microchannel module, a hydrogen flux of 195.3 $mL \cdot min^{-1} \cdot cm^{-2}$ is obtained at 450 °C and 5 bars feed pressure, corresponding to a permeability of $3.4 \cdot 10^{-8}$ $mol \cdot m^{-1} \cdot s^{-1} \cdot Pa^{-0.5}$. During the complete operation of 1100h at 450 °C, the module shows a very good stability up to the highest feed pressure applied of 15 bars. The N_2 leakage flux has remained below the detection limit of the equipment, 5 $\mu L \cdot cm^{-2} \cdot min^{-1}$, resulting in a minimum value for the H_2/N_2 permselectivity of 39.000 applying the pure H_2 flux value obtained at 5 bars.

Keywords: palladium-silver membrane; magnetron sputtering; microchannel module; stability investigation; hydrogen flux; selectivity.

1. Introduction

Palladium (Pd) and many Pd-alloys have high solubility and diffusivity of hydrogen, and are therefore promising as membranes for medium to high temperature hydrogen separation (250–550°C) [1, 2]. Compared to other types of hydrogen separation membranes [2], Pd-based membranes provide the best hydrogen flux-selectivity combination, and possible applications are typically found in hydrogen production, recovery and purification [1, 3-8], hydrogenation [9] and dehydrogenation [9, 10] processes. Current membrane technology comprises self-supported and mechanically supported composited structures. Self-supported membranes are usually tubes or foils with thickness range of 50–100 μm with thicker membranes used at higher total trans-membrane pressure [11]. To reduce cost and increase flux, composite membranes consisting of membranes of 2–10 μm thickness deposited on porous steel or ceramics are being developed [1]. Composite membranes have successfully been operated at laboratory scale and small pilot scale producing hydrogen for up to 13.000 hours [12], and the technology appears ready for up-scaling. However, operation of these high-performing Pd-based membranes has made external mass transfer limitations, or concentration polarization, due to depletion of H_2 in the gas-phase layer next to the membrane surface critically important for some module designs and operating conditions [13-15]. This reduces the efficient partial pressure of hydrogen, and thereby also the pressure gradient sustaining the hydrogen flux. For example, the obtained H_2 flux in the world's largest scale membrane reformer equals only 50% of the flux value assuming bulk diffusion of hydrogen through the Pd membrane as rate determining step [16, 17]. The main cause of the flux reduction is believed to be concentration polarization [13, 18].

These gas phase limitations can only be reduced by smart membrane and module design in order to optimize feed flow conditions to reduce the thickness of the hydrogen-depleted layer. Microstructured membrane reactors that reduce gas phase diffusion limitations and increase the membrane area to reactor volume ratio compared to traditional tubular reactors, offer in this respect great advantages. Since concentration polarization effects are expected to be subordinate, a high space–time-yield is anticipated due to the supplied high volumetric surface area for reaction and membrane separation.

We have previously reported on the integration of thin unsupported Pd-Ag films in microchannel-configured devices that drastically reduce the distance between the bulk of the feed gas and the Pd membrane surface to the sub-millimetre region thereby reducing concentration polarization effects. For example, membrane modules have been fabricated where the thin Pd-Ag films are simply clamped between polished microchannel-configured flanges. For moderate trans-membrane pressure difference, *i.e.*, up to 1 – 3 bars, and for temperatures not higher than 400 °C, microchannels with a width between 200 μm and 1000 μm provided sufficient mechanical support even for the thinnest membranes tested, down to 1.4 μm [19]. Moreover, mixed gas permeation experiments revealed that concentration polarization effects are expected to be subordinate [20]. Along the same line, all-metallic membrane modules with micro-machined plates directly attached to the membrane by laser welding have been fabricated by the Karlsruhe Institute of Technology (KIT) applying the SINTEF thin free-standing films [20]. This is considered to be a very practical approach, and represents a first step towards a compact multi-layered microchannel membrane reformer system. In this work, membrane stability was achieved up to at least 4.5 and 3 bars for 13 and 4.7 micron thick $Pd_{77}Ag_{23}$ membranes, respectively [20]. The maximum bursting pressure was never reached during the experiments showing that the microchannels serve as a good support for the palladium membranes. The long-term stability for these microchannel membrane modules, however, has not been reported to our knowledge.

In the present work, we report a more thorough investigation of the long-term stability of various designs of microstructured membrane modules. In all modules, a microchannel-configured feed section is applied consisting either of 200 or 1000 micron-wide channels. On the permeate side, a stainless steel plate with apertures corresponding to the channel geometry, or a porous stainless steel (PSS) for application at higher feed pressures is applied. In the experiments, the H_2 permeation performance and stability of the modules are verified over a period of up to 50 days, while systematically increasing both temperature and pressure. Tested microstructured membrane modules are characterised employing different techniques, including scanning electron microscopy (SEM), energy dispersive spectroscopy (EDS), and white light interferometry (WLI).

2. Experimental

2.1 Experimental

$Pd_{77}Ag_{23}$ films were prepared using a CVC 601 magnetron sputtering apparatus. The membranes were sputtered from a $Pd_{77}Ag_{23}$ target onto silicon single crystal substrates. The vacuum chamber was pumped down before introducing the sputtering gas Ar (99.9999%) into the system. Membrane films with a nominal thickness of 10 micron were applied in the current work.

2.2 Film integration in various membrane module configurations

After sputtering and removal from the silicon wafer, the free-standing $Pd_{77}Ag_{23}$ film has been integrated in various membrane module configurations. The membrane growth side from the sputtering process was always placed facing the feed housing of the apparatus, while the side that faced the substrate always faced the permeate side.

A stainless steel plate with apertures corresponding to the channel geometry, or alternatively, porous stainless supports, can be employed for mechanical support. In all microchannel modules employed in this study, a microchannel-configured feed section has been applied consisting either of 200 or 1000 micron-wide and deep channels. The 200 micron-wide micro-channel system consisted of fifteen channels machined with dimensions 0.2 x 0.2 x 13 mm, providing for a 0.39 cm^2 active membrane area. In addition, the circular gas inlet and outlet areas with a diameter of 500 μm provided an area of 0.059 cm^2, giving a total effective area for permeation of 0.449 cm^2. The 1000 micron-wide micro-channel system consisted of seven parallel channels machined with dimensions 1 x 1 x 13 mm^3, providing in total for a 0.91 cm^2 active membrane area. This area was applied in the calculation of flux, permeance and permeability. On the permeate side, a stainless steel plate with apertures corresponding to the channel geometry, or a porous stainless steel for application pressures above 5 bars have been applied (SIKA-R1, 1 micron rating supplied GKN Sinter Metals, Germany). The thickness of the porous support was 3 mm, while the employed microchannel-configured support plate had a thickness of 1 mm. More information on the applied modules can be found here [15, 19, 20].

2.3 H_2 permeation measurements

Sealing was performed by clamping the Pd film between the feed and permeate section of the microchannel module, both which were highly polished with 3μm SiC particles before mounting. At the start-up of every experiment the N_2 leakage flux, obtained at room temperature applying 4 bar of nitrogen pressure, remained below the detection limit of the gas chromatograph (Varian Inc., CP-4900) analysis, 5 $\mu L \cdot cm^{-2} \cdot min^{-1}$, confirming that the sealing process was successful, and that all applied Pd films have a very low defect density, and are virtually free of any leakage flux.

H_2 permeation experiments were conducted using custom-made permeation equipment. Automated mass flow controllers (Bronkhorst High-Tech) were used to control the gas supply to the feed and permeate sides of the membrane. When heating up the module, the membrane was flushed with N_2 (99.999%) and Ar (99.999%) on the feed and permeate side, respectively, until 300 °C was reached. Then H_2 (99.995%) was introduced at the feed side. In order to follow the appearance of leakage through the membrane, the H_2 permeability of the prepared films was obtained applying a feed gas mixture of H_2 in N_2. A sweep flow of Ar (99.999%) was applied at the permeate side. To prevent the consumption of large amounts of gas during the long-term experiments, the feed and sweep flow rate are equal to 200 and 50 $NmL \cdot min^{-1}$, respectively. Note that the obtained H_2 flux from these experiments are thus low and do not reflect the capability of the membranes, as the H_2 flux is limited by depletion and remaining concentration polarization effects [20]. Typically, the experiments are run under a hydrogen recovery factor of 40–50%. The H_2 flux was calculated from the measured hydrogen concentration in the permeate using the calibrated flow of Ar sweep gas. For this the permeate composition was monitored by GC measurements (Varian Inc., CP-4900, equipped with a thermal conductivity detector (TCD)).

2.4 Post-process characterisation

The membrane appearance was investigated after the H_2 permeation measurements using white light interferometry (WLI) (Veeco Instruments Inc., Wyko NT9800). The microstructure of the membranes were characterised using scanning electron microscopy (SEM) (FEI, NanoSEM 650) combined with energy dispersive spectroscopy (EDS) (Oxford Instruments, X-MAX50).

3. Results and discussion

3.1 Microchannel-supported $Pd_{77}Ag_{23}$ membrane modules

3.1.1 1000 micron-wide microchannel modules

Figure 1 shows the H_2 permeation properties and membrane-module stability at 500 °C and 4 bars for 1300h, during a typical experiment initially starting at an operating temperature of 400 °C, which was gradually increased to 500 °C during the initial 300h.

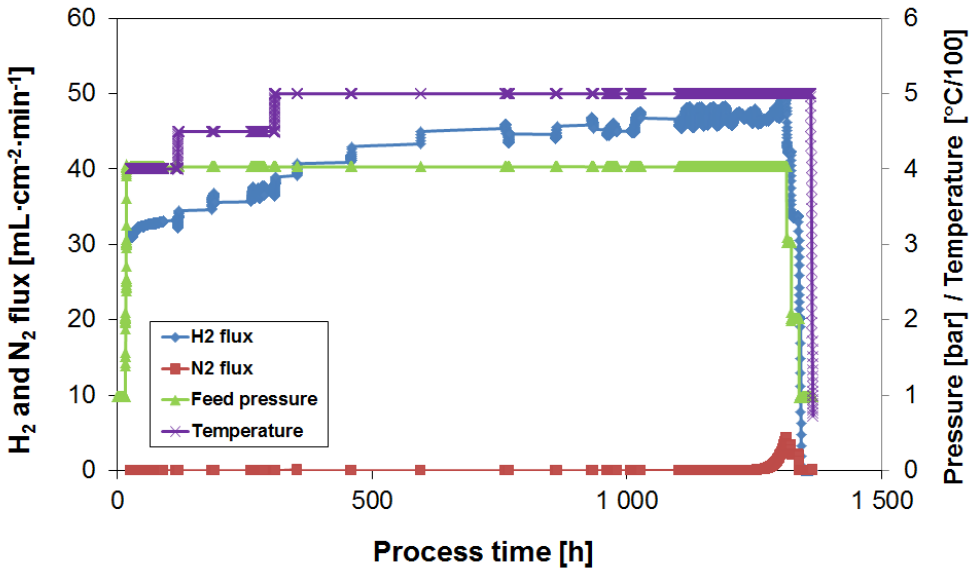

Figure 1 H_2 and N_2 flux during operation of 1300h up to 500 °C and 4 bars, respectively. Feed applying 60% H_2 in N_2 at 200 NmL·min^{-1}, Ar sweep flow rate at 50 NmL·min^{-1}.

From the start-up of the experiment at 400 °C and 4 bars, a gradually increasing H_2 flux is obtained. The increase in operating temperature to 450 °C and subsequently to 500 °C evokes an acceleration of the H_2 flux increase, see Figure 1. For example, an increase in H_2 flux from 41 to 45 mL·cm^{-2}·min^{-1} is observed between a process time of 500 and 1000h. This is presumably due to a deformative settling (as shown later) of the Pd film into the micro-channel permeate section that leads to a reduction in membrane thickness, combined with an increase in the effective area for permeation, both resulting in an increasing H_2 flux. Note, however, that the settling does not result in an increase in unselective flow of N_2. The obtained separation factor obtained after

800h of operation equals 40,000. However, ultimately this behaviour results in the membrane failure observed after 1300h as indicated by the rapid increase in N_2 leakage flux and a rapid decrease in separation factor to below 100.

Figure 2 shows the deflection of the $Pd_{77}Ag_{23}$ film into the microchannel support as visualised with white light interferometry (WLI). The WLI results show that the film has deflected as much as between 250 and 400 µm into the 1000 µm wide microchannels, depending on the axial position in the channel. This corresponds roughly to an increase in the effective area for permeation of 35%. Note that it is difficult to assess this from the permeation measurements as experiments are performed at a relative low feed flow rate. Moreover, the curvature in the WLI measurement at y = 0 shows that the microchannel-configured support plate has bended slightly during the long-term operation at these operating conditions.

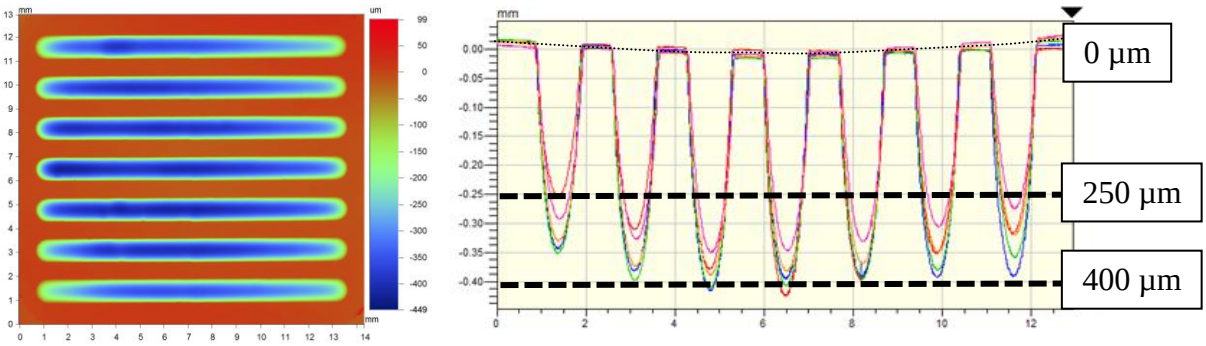

Figure 2 (a) White light interferometry (WLI) image of the microchannel permeate section, the colours give an indication of the depth; (b) WLI line scan across the 7 microchannels with a width of 1mm, showing the depth of deformation of the film into the channels at different axial positions.

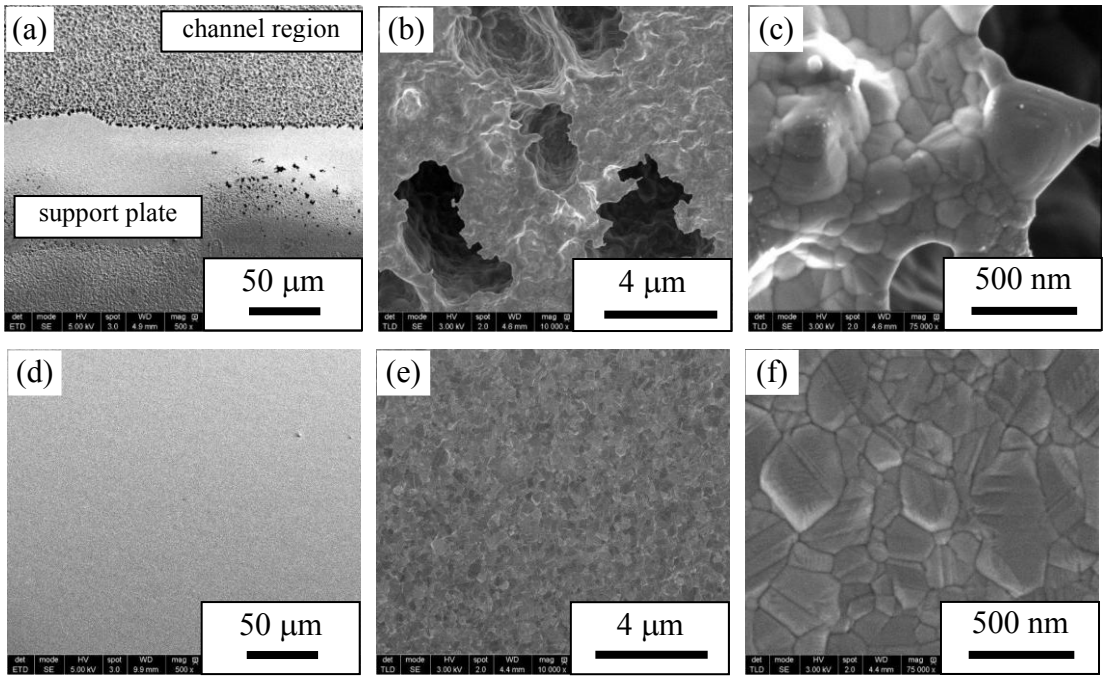

Figure 3 SEM images with varying magnifications of the membrane film after testing: (a–c) feed surface, 3(b) and (c) shows magnified images of the channel region of the feed surface; (d–f) permeate surface.

Figure 3 shows SEM micrographs of the feed and permeate of the tested membrane film. Figure 3(a) clearly shows the imprint of microchannels across the $Pd_{77}Ag_{23}$ film. A further examination of the supported film also shows that a porosity has appeared on the membrane feed surface during the testing, see Figure 3(b-c). The elevated operation pressure allows the material to deform through plastic deformation, which apparently lead to microstructural changes and finally pore formation during the deformative settling in the channels [21]. Figure 3(b) shows pores, or a porosity, with a diameter of about 4 μm evenly distributed over the free-standing feed surface of the membrane. In addition to the settling of the film into the channels, the observed surface porosity leads to an increased membrane surface area which is available for hydrogen dissociation. As shown previously [22-24], air-treated membranes develop structural changes, *i.e.* void formation and surface roughening. In some cases, voids, which form near the membrane surface region, grow as big as 200 nm and emerge to the surface where they turn into pits [22]. However, this cannot be the cause for the currently observed surface porosity as these membranes are not exposed to air at operating temperature.

SEM micrographs taken from the permeate side of the membrane, however, do not show any evidence of pore formation. The observed pores on the feed side thus do not penetrate through the whole thickness of the membrane as also verified by the high separation factor during the experiment. On the permeate side, the grain size roughly equals 200–400 nm. As a comparison, grains with a size of around 200 nm are observed after long-term operation of a $Pd_{77}Ag_{23}$ membrane supported on porous stainless steel tubes, on-average just a factor of approximately two larger than that of as-grown samples [25]. Enhanced grain growth is thus occurring under the present membrane operation at a somewhat higher operating temperature, although this does not lead to dramatic changes in the permeate side microstructure. The membrane failure is most probably related to crack formation in the $Pd_{77}Ag_{23}$ film, and on the feed surface membrane one large crack is observed, see Figure 4.

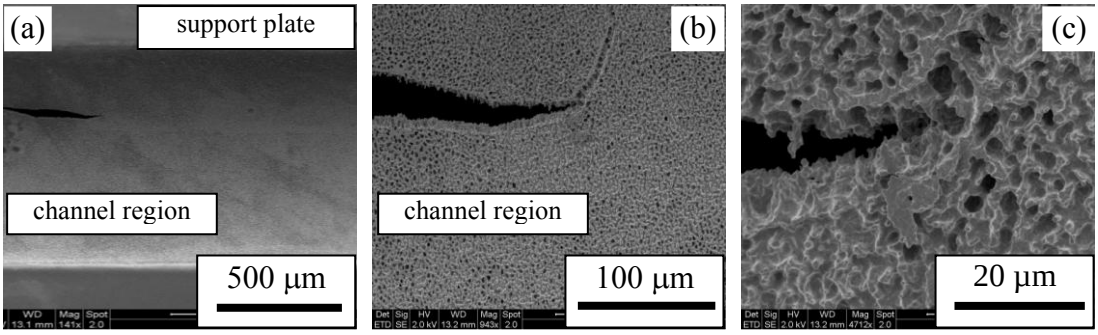

Figure 4 SEM images with varying magnifications of the crack area observed on the membrane surface after testing.

In an effort to verify the membrane module stability at a somewhat lower operating temperature, a new experiment was started limiting the operating temperature to 450 °C. Figure 5 shows the H_2 permeation properties and membrane-module stability at 450 °C, during an experiment initially starting at a feed pressure of 2 bars, which was gradually increased to 6 bars over a period of 1300h.

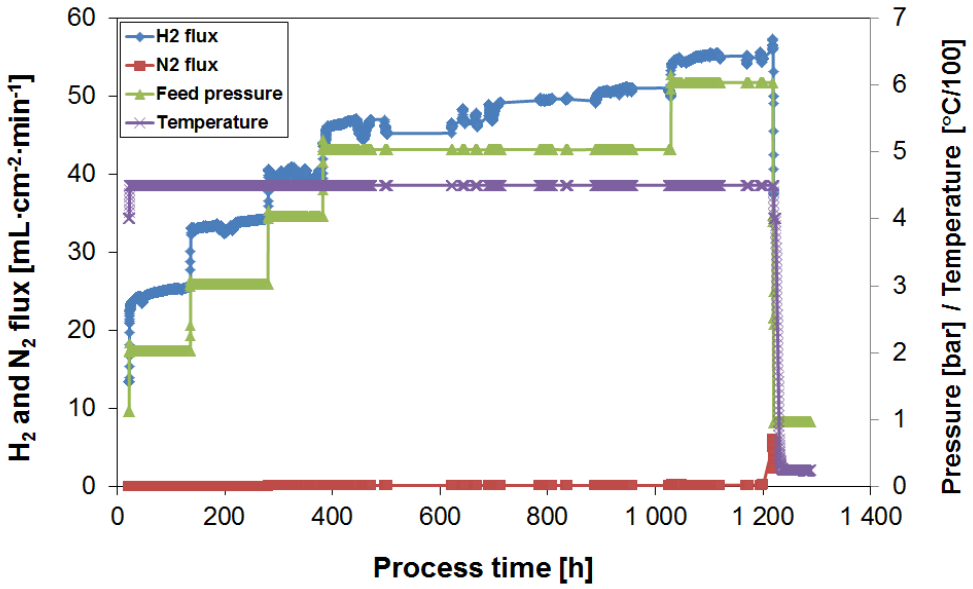

Figure 5 H_2 and N_2 flux during operation of 1200h up to 450 °C and 6 bars, respectively. Feed applying 60% H_2 in N_2 at 200 NmL·min^{-1}, Ar sweep flow rate at 50 NmL·min^{-1}.

A relatively stable operation is obtained at 450 °C at 2, 3 and 4 bar feed pressure during the first 400h of operation. However, again a gradually increasing H_2 flux is obtained at 5 bars. For example, an increase in H_2 flux from 46 to 51 mL·cm^{-2}·min^{-1} is observed during 600h of operation. Within 200h after the subsequent increase in feed pressure to 6 bars, a membrane failure is again observed after a total process time of 1200h. This failure was provoked by a sudden fluctuation in gas supply that most probably cracked the membrane film in the same way as shown in Figure 4.

The post-process characterisation shows a similar behaviour as the membrane operated up to 500 °C: we again observe a large settling of the film into the permeate section combined with microstructural changes on the feed surface of the membrane. Similarly, no microstructural changes and pinhole formation are seen on the membrane permeate side (results not shown). Based on the described long-term experiments and related stability at varying operating conditions, the operation of the 1mm wide microchannel membrane modules is tentatively limited to a temperature and pressure of 400 °C and 5 bars, respectively. Next, the membrane stability employed in 200 micron-wide microchannel support modules is reported.

3.1.2 200 micron-wide microchannel modules

Figure 6 shows the H_2 permeation properties and membrane-module stability up to 550 °C, during an experiment initially starting at a feed pressure of 5 bars, which was increased to 6 bars at a process time of 90h.

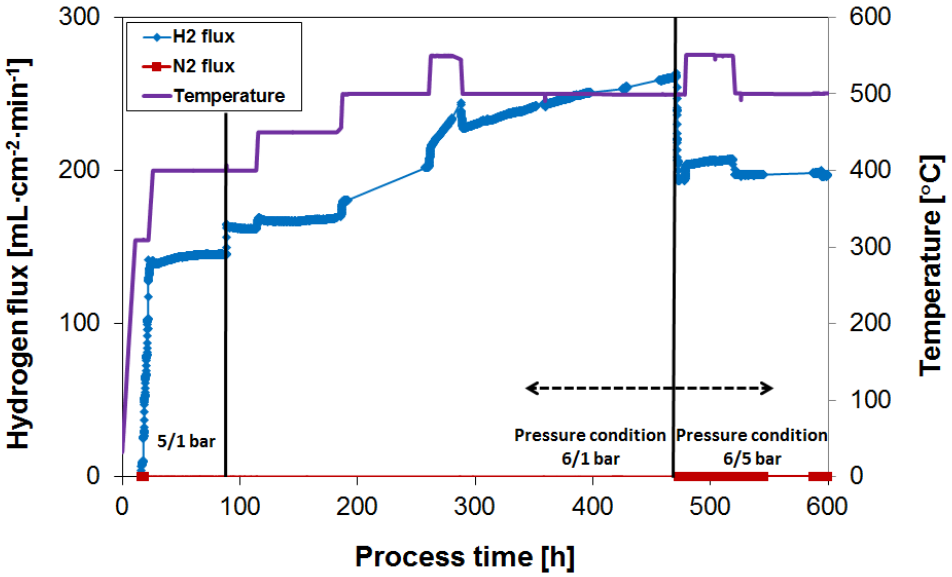

Figure 6 H_2 and N_2 flux during operation of 600h up to 550 °C and 6 bars, respectively. Feed applying 80% H_2 in N_2 at 200 NmL·min^{-1}, Ar sweep flow rate at 50 NmL·min^{-1}.

A relatively stable H_2 flux is obtained at 400 and 450 °C during 200h of operation, however, a gradually increasing H_2 flux is obtained at 500 and 550 °C. For example, a H_2 flux increase from 217 to 230 mL·cm^{-2}·min^{-1} is observed during half a day of operation at 550 °C. Again, this is presumably due to a deformative settling of the Pd film into the micro-channel permeate section. Note that the settling again not results in unselective flow of N_2, not even after an additional 200h of operation at a temperature and pressure of 500 °C and 6 bars, respectively. Stable operation has been obtained by increasing the permeate side pressure to 5 bars, while keeping the feed side at 6 bars, thereby decreasing the absolute pressure drop over the membrane. The post-process characterisation by SEM shown in Figure 7 proves the dramatic deformative settling of the $Pd_{77}Ag_{23}$ film also for the case of the 200 micron wide micro-channel support.

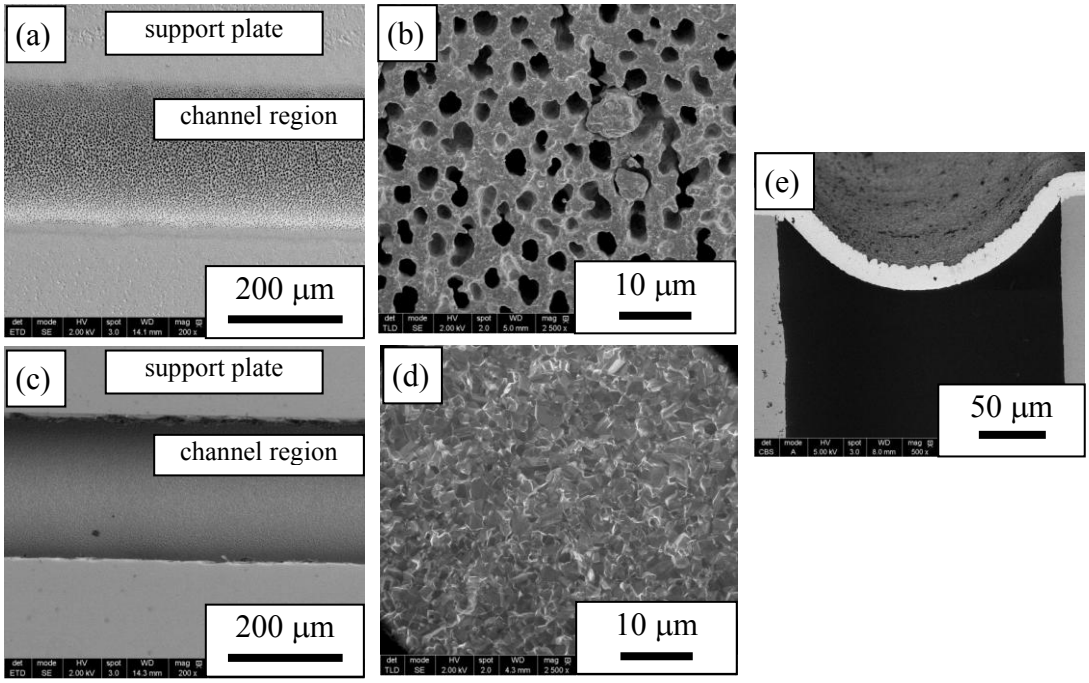

Figure 7 SEM micrographs of a 12.5 micron-thick $Pd_{77}Ag_{23}$ film applied in microchannel module with channel dimensions of 200 µm tested for 53 days up to a temperature and pressure of 550 °C and 6 bars, respectively (a) feed side, magnification 200x; (b) feed side of the channel region, magnification 2500x; (c) permeate side, magnification 200x; (d) permeate side of the channel region, magnification 2500x; (e) cross-section, magnification 500x.

The imprints of the microchannels are clearly visible through the $Pd_{77}Ag_{23}$ film, see Figure 7(a), while the supported film also shows the presence of pores, or a structural porosity, with a diameter of about 2 µm evenly distributed over the whole feed surface, see Figure 7(b). As was observed for the 1000 µm wide microchannel modules, it might seem obvious that these pores cause a direct membrane leakage, however, SEM micrographs taken from the permeate side of the membrane show that little microstructural changes and pore formation has occurred, and that the observed pores on the feed side thus do not penetrate through the whole thickness of the membrane. SEM micrographs of the cross-section of the tested membrane are shown in Figure 7(e), showing a deflection of around 65 µm. WLI results show that the film is roughly deflected 50 – 75 µm varying over the channel length. Due to the settling the available membrane cross-sectional perimeter has increased with roughly 22.5% to 245 µm (value obtained by measuring the area from Figure 7(e)).

Even though a slight membrane thickness variation is observed in the cross-section SEM picture, a thickness roughly equal to 10 μm is obtained comparison with the thickness of the as-prepared film which equals 12.5 μm. Based on the cross-section thickness measurements it can therefore be concluded that a thickness reduction equal to 20% has occurred during the testing. This corresponds fairly well with the extent of membrane area increase due to the settling. Note that the depth of the settling, as well as the pore size of the porosity formed is less than for the 1000 μm wide channels discussed previously. However, it is reasonable to believe that also the operation of the 200 micron-wide microchannel under the current operating conditions ultimately leads to a membrane failure. For pressures above 5 bars, the application of microchannel-supported modules is thus not possible, and continuous porous metallic or ceramic supports are required for sufficient stabilisation of the thin $Pd_{77}Ag_{23}$ films. The performance and long-term stability of these porous stainless steel-supported $Pd_{77}Ag_{23}$ membrane modules employing a microchannel-configured feed section is discussed in the following.

3.2 Porous stainless steel-supported $Pd_{77}Ag_{23}$ membrane modules

In Figure 8 we first give the H_2 flux obtained at 450 °C applying pure hydrogen as feed as a function of the hydrogen partial pressure difference. No active sweep was applied during these measurements. At 5 bar feed pressure, a hydrogen flux of 195.3 $mL \cdot min^{-1} \cdot cm^{-2}$ was obtained, corresponding to a permeability of $3.4 \cdot 10^{-8}$ $mol \cdot m^{-1} \cdot s^{-1} \cdot Pa^{-0.5}$. In the permeability calculation the *n*-value is forced to 0.5, however, a best fit between the H_2 flux and $\left(p_{H_2^{ret}}^n - p_{H_2^{perm}}^n\right)$ has been obtained using a value of *n* equal to 0.55. The H_2 permeability obtained for the membrane applied in this study corresponds well with values obtained for tubular Pd–23%Ag/stainless steel composite membranes [26]. The activation energy of the permeation through the membrane obtained between 300 and 450 °C at a pressure of 3 bars equals 6.6 $kJ \cdot mol^{-1}$, close to reported values for $Pd_{77}Ag_{23}$ membranes [27].

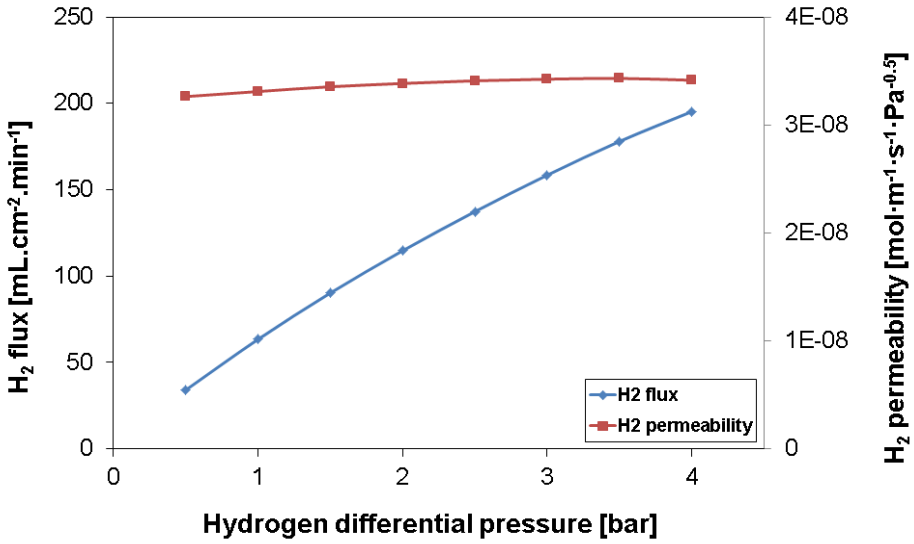

Figure 8 Hydrogen permeation flux obtained using pure hydrogen as feed as a function of the hydrogen partial pressure difference at T = 450 °C. Permeate at atmospheric pressure, no sweep applied. Measurements performed after the flux stabilisation up to a feed pressure of 6 bars.

Figure 9 shows the H_2 permeation properties of the PSS-supported membrane module at 450 °C, during a long-term stability investigation experiment during which the feed pressure has been increased step-wise to 15 bars over a period of 1100h.

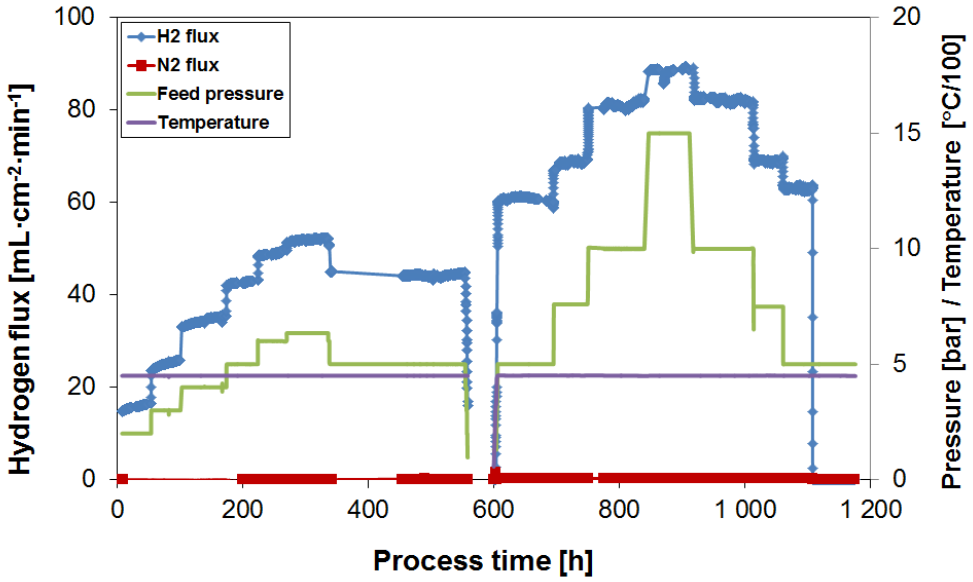

Figure 9 H_2 and N_2 flux during operation of 1100h up to 15 bars at an operating temperature of 450 °C, respectively. Feed applying 60% H_2 in N_2 at 200 NmL·min^{-1},

Ar sweep flow rate at 50 $NmL \cdot min^{-1}$. Between a process time of 550 and 600h, the module was moved to another experimental set-up that allowed for higher feed pressures.

From Figure 9 it can be seen that the module shows a very good stability up to the verified feed pressure of 15 bars. After the initial settling of the $Pd_{77}Ag_{23}$ film into the porous stainless steel support for feed pressures up to 6 bars, during which the H_2 flux shows an increasing behaviour at constant operating pressure, the H_2 flux remains constant at constant pressure. During the complete process time of 1100h, the N_2 leakage flux remains below the detection limit of the equipment, 5 $\mu L \cdot cm^{-2} \cdot min^{-1}$, resulting in a minimum value for the H_2/N_2 permselectivity of 39,000 applying the pure H_2 flux value obtained at 5 bars. After 1100h, the experiment was aborted and the membrane module was made available for post-process characterisation. Figure 10 and 11 show SEM micrographs obtained from the membrane surface and cross-section, respectively.

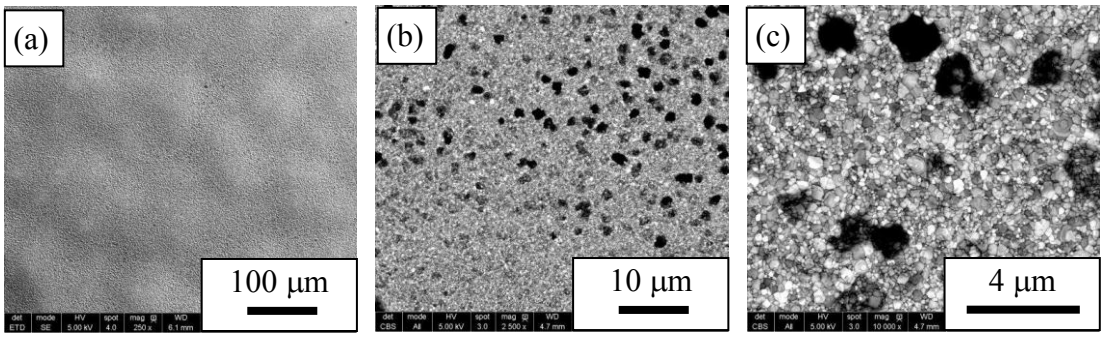

Figure 10 SEM micrographs obtained of the 10 micron-thick $Pd_{77}Ag_{23}$ membrane surface as applied in a porous stainless steel supported module after operation of 1100h.

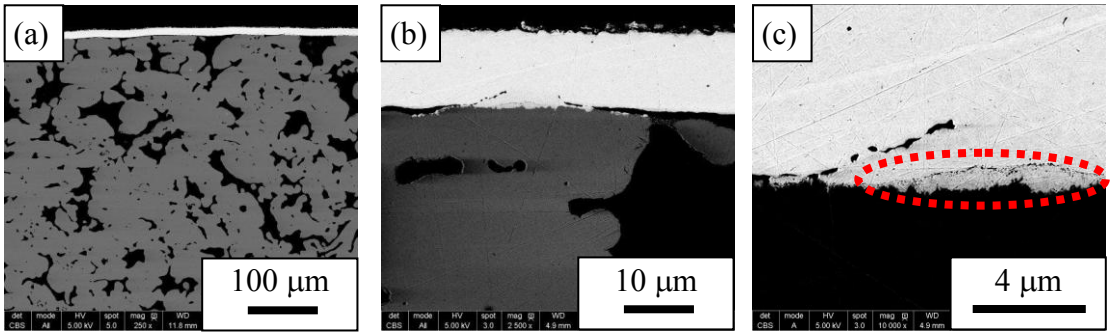

Figure 11 Cross-section SEM micrographs obtained of the 10 micron-thick $Pd_{77}Ag_{23}$ membrane as applied in a porous stainless steel supported module after operation of 1100h, (a) and (b) $Pd_{77}Ag_{23}$ membrane film supported by the porous stainless steel support; (c) Magnification of the $Pd_{77}Ag_{23}$-steel interface.

The topography of the feed surface shown in Figure 10(a) contains some bulged areas which are almost uniformly spread throughout the membrane. These bulged areas have been formed on the membrane surface while following the surface topography of the porous support during the high pressure operation. From Figure 10(c) it is seen that pores are formed in the surface. These pores are formed most probably where the film deformation is largest. The pore size, as appearing from the feed side, is about 2 µm showing that the pores do not penetrate the whole membrane thickness. This is as well verified by the N_2 leakage flux that remained below the detection limit of the equipment throughout the experiment. However, their growth behaviour and effect on the long-term stability of the membrane requires further investigation. In addition, some expected intermetal diffusion was confirmed using SEM-EDS, see Figure 11(c). In between the PSS support and the $Pd_{77}Ag_{23}$ film, a secondary phase has formed with an approximate composition of 63 at.% Pd, 25 at.% Fe, 7 at.% Cr, 5 at.% Ni, and no evidence for Ag. However, even up to an operation time of 1100h at 450°C the intermetal diffusion has reached less than 1 micron, and does not have large negative effects on the operational stability of this membrane module.

4. Conclusions

The long-term stability over a period of up to 50 days has been reported for various designs of microstructured $Pd_{77}Ag_{23}$ membrane modules for H_2 production and purification. In all modules, a microchannel-configured feed section has been applied

consisting of either 200 or 1000 micron-wide channels. On the permeate side, a stainless steel plate with apertures corresponding to the channel geometry or a porous stainless steel have been applied. Even though microchannels with a width between 200 µm and 1000 µm provide sufficient mechanical support for moderate trans-membrane pressure difference, *i.e.*, up to approximately 5 bars, and for temperatures less than approximately 400 °C, long-term operation under these operating conditions results in a large deformative settling of the $Pd_{77}Ag_{23}$ film into the microchannel support. The elevated operation pressure allows the material to deform through plastic deformation, which apparently leads to microstructural changes during the deformative settling in the channels. Ultimately this behaviour results in membrane failure. The deformation is more extensive and the pores formed are larger for the 1000 µm compared to the 200 µm channels. For pressures above 5 bars, the application of microchannel-supported modules is thus not feasible, and for that purpose a continuous porous stainless steel support is introduced that allows for a stabilisation of the thin $Pd_{77}Ag_{23}$ films up to the maximum applied pressure of 15 bars. For such a porous stainless steel supported microchannel module, a hydrogen flux of 195.3 $mL \cdot min^{-1} \cdot cm^{-2}$ was obtained at 450 °C and 5 bars feed pressure, corresponding to a permeability of $3.4 \cdot 10^{-8}$ $mol \cdot m^{-1} \cdot s^{-1} \cdot Pa^{-0.5}$. The module showed very good stability over 1100h with a N_2 leakage flux remaining below the detection limit of the equipment, 5 $\mu L \cdot cm^{-2} \cdot min^{-1}$, resulting in a minimum value for the H_2/N_2 permselectivity of 39,000. Post-process characterisation, however, showed pore formation in the feed side film surface. Their growth behaviour and effect on the long-term stability of the membrane requires further investigation.

Acknowledgements

The financial support from the Research Council of Norway (RCN) through the following programs, RENERGI (Project No: 216056/E20), and CLIMIT (Contract No. 215666/E20), and the FCH-JU ReForCELL project, (Contract no.: 278997) (http://reforcell.eu/) are gratefully acknowledged.

References

[1] S.N.Paglieri, J.D.Way, Innovations in palladium membrane research, Separation and Purification Methods 31 (2002) 1-169.

[2] N.W.Ockwig, T.M.Nenoff, Membranes for hydrogen separation, Chem. Rev. 107 (2007) 4078-4110.

[3] G.Q.Lu, J.C.Diniz da Costa, M.Duke, S.Giessler, R.Socolow, R.H.Williams, T.Kreutz, Inorganic membranes for hydrogen production and purification: A critical review and perspective, Journal of Colloid and Interface Science 314 (2007) 589-603.

[4] T.M.Nenoff, R.J.Spontak, C.M.Aberg, Membranes for hydrogen purification: An important step toward a hydrogen-based economy, Mrs Bulletin 31 (2006) 735-741.

[5] G.Chiappetta, G.Clarizia, E.Drioli, Design of an integrated membrane system for a high level hydrogen purification, Chemical Engineering Journal 124 (2006) 29-40.

[6] G.J.Grashoff, C.E.Pilkington, C.W.Corti, Purification of hydrogen, Platinum Metals Review 27 (1983) 157-169.

[7] D.L.McKinley, US Patent 3,439,474, 22-4-1969

[8] D.L.McKinley, US Patent 3,350,845, 7-11-1967

[9] R.Dittmeyer, V.Hollein, K.Daub, Membrane reactors for hydrogenation and dehydrogenation processes based on supported palladium, Journal of Molecular Catalysis A: Chemical 173 (2001) 135-184.

[10] J.P.Collins, R.W.Schwartz, R.Sehgal, T.L.Ward, C.J.Brinker, G.P.Hagen, C.A.Udovich, Catalytic dehydrogenation of propane in hydrogen permselective membrane reactors, Ind. Eng. Chem. Res. 35 (1996) 4398-4405.

[11] S.Tosti, L.Bettinali, V.Violante, Rolled thin Pd and Pd/Ag membranes for hydrogen separation and production, International Journal of Hydrogen Energy 25 (2000) 319-325.

[12] H.Yakabe, Operations of a 40 Nm3/h-class Membrane Reformer System at Tokyo Gas, Presentation at the International Joint Workshop on Palladium Membrane Technology - Rome, Italy 12-14 November (2012).

[13] T.A.Peters, M.Stange, H.Klette, R.Bredesen, High pressure performance of thin Pd-23%Ag/stainless steel composite membranes in water gas shift gas mixtures; influence of dilution, mass transfer and surface effects on the hydrogen flux, Journal of Membrane Science 316 (2008) 119-127.

[14] A.Caravella, G.Barbieri, E.Drioli, Concentration polarization analysis in self-supported Pd-based membranes, Separation and Purification Technology 66 (2009) 613-624.

[15] A.L.Mejdell, T.A.Peters, M.Stange, H.J.Venvik, R.Bredesen, Performance and application of thin Pd-alloy hydrogen separation membranes in different configurations, Journal of the Taiwan Institute of Chemical Engineers 40 (2009) 253-259.

[16] A.Unemoto, A.Kaimai, K.Sato, T.Otake, K.Yashiro, J.Mizusaki, T.Kawada, T.Tsuneki, Y.Shirasaki, I.Yasuda, Surface reaction of hydrogen on a palladium alloy membrane under co-existence of H2O, CO, CO2 or CH4, International Journal of Hydrogen Energy 32 (2007) 4023-4029.

[17] A.Unemoto, A.Kaimai, K.Sato, T.Otake, K.Yashiro, J.Mizusaki, T.Kawada, T.Tsuneki, Y.Shirasaki, I.Yasuda, The effect of co-existing gases from the process of steam reforming reaction on hydrogen permeability of palladium alloy membrane at high temperatures, International Journal of Hydrogen Energy 32 (2007) 2881-2887.

[18] H.Kurokawa, H.Yakabe, I.Yasuda, T.Peters, R.Bredesen, Inhibition effect of CO on hydrogen permeability of Pd–Ag membrane applied in a microchannel module configuration, International Journal of Hydrogen Energy 39 (2014) 17201-17209.

[19] A.L.Mejdell, M.Jøndahl, T.A.Peters, R.Bredesen, H.J.Venvik, Experimental investigation of a microchannel membrane configuration with a 1.4 micron Pd/Ag23wt.% membrane: effects of flow and pressure, Journal of Membrane Science 327 (2009) 6-10.

[20] T.Boeltken, M.Belimov, P.Pfeifer, T.A.Peters, R.Bredesen, R.Dittmeyer, Fabrication and testing of a planar microstructured concept module with integrated palladium membranes, Chemical Engineering and Processing: Process Intensification 67 (2013) 136-147.

[21] W.Mekonnen, B.Arstad, H.Klette, J.C.Walmsley, R.Bredesen, H.Venvik, R.Holmestad, Microstructural characterization of self-supported 1.6 [mu]m Pd/Ag membranes, Journal of Membrane Science 310 (2008) 337-348.

[22] W.Tucho, H.Venvik, J.Walmsley, M.Stange, A.Ramachandran, R.Mathiesen, A.Borg, R.Bredesen, R.Holmestad, Microstructural studies of self-supported (1.5 to 10 um) Pd/23-wt%Ag hydrogen separation membranes subjected to different heat treatments, Journal of Materials Science 44 (2009) 4429-4442.

[23] F.Guazzone, E.E.Engwall, Y.H.Ma, Effects of surface activity, defects and mass transfer on hydrogen permeance and n-value in composite palladium-porous stainless steel membranes, Catalysis Today 118 (2006) 24-31.

[24] F.Roa, J.D.Way, The effect of air exposure on palladium-copper composite membranes, Applied Surface Science 240 (2005) 85-104.

[25] T.A.Peters, W.M.Tucho, A.Ramachandran, M.Stange, J.C.Walmsley, R.Holmestad, A.Borg, R.Bredesen, Thin Pd-23%Ag/stainless steel composite membranes: Long-term stability, life-time estimation and post-process characterisation, Journal of Membrane Science 326 (2009) 572-581.

[26] T.A.Peters, M.Stange, R.Bredesen, On the high pressure performance of thin supported Pd-23%Ag membranes--Evidence of ultrahigh hydrogen flux after air treatment, Journal of Membrane Science 378 (2011) 28-34.

[27] W.M.Tucho, H.J.Venvik, M.Stange, J.C.Walmsley, R.Holmestad, R.Bredesen, Effects of thermal activation on hydrogen permeation properties of thin, self-supported Pd/Ag membranes, Separation and Purification Technology 68 (2009) 403-410.